Deciphering Intrinsic Deactivation/Isomerization Routes in a Phytochrome Chromophore Model

Piero Altoè,[†] Teresa Climent,[‡] Giulia C. De Fusco,[§] Marco Stenta,[†] Andrea Bottoni,[†] Luis Serrano-Andrés,[‡] Manuela Merchán,*[,‡] Giorgio Orlandi,[†] and Marco Garavelli*[,†]

Dipartimento di Chimica "G. Ciamician", Università di Bologna, Via Selmi 2, Bologna I-40126, Italy, Instituto de Ciencia Molecular, Universitat de València, ES-46071 Valencia, Spain, and Department of Chemistry, Thomas Young Centre, Imperial College London, South Kensington Campus, London SW7 2AZ, U.K.

Received: April 1, 2009

High level ab initio correlated (CASPT2) computations have been used to elucidate the details of the photoinduced molecular motion and decay mechanisms of a realistic phytochrome chromophore model in vacuo and to explore the reasons underneath its photophysical/photochemical properties. Competitive deactivation routes emerge that unveil the primary photochemical event and the intrinsic photoisomerization ability of this system. The emerged in vacuo based static (i.e., nondynamical) reactivity model accounts for the formation of different excited state intermediates and suggests a qualitative rationale for the short (picosecond) excited state lifetime and ultrafast decay of the emission, its small quantum yield, and the multiexponential decay observed in both solvent and phytochromes. It is thus tentatively suggested that this is a more general deactivation scheme for photoexcited phytochrome chromophores that is independent of the surrounding environment. Spectroscopic properties have also been simulated in both isolated conditions and the protein that satisfactorily match experimental data. For this purpose, preliminary hybrid QM/MM computations at the correlated (CASPT2) level have been used in the protein and are reported here for the first time.

1. Introduction

Phytochromes (phys) are a large and heterogeneous family of red and far-red photoreceptors present in eukaryotes and prokaryotes that can switch between two photoconvertible forms, P_r and P_{fr} (see Scheme 1).[1] This light-induced transition initiates transcriptional signaling cascades that regulate plant growth and development and is responsible for fundamental functions that spread from the control of phototaxis and pigmentation in bacteria to seed germination and shade avoidance in plants.[1] The three chromophores found in phys (phytochromobilin (PΦB), biliverdin (BV), and phycocyanobilin (PCB)) are very similar and share a linear fully conjugated tetrapyrrolic system with differences on the first (A) and last (D) rings (see Scheme 2). Their photophysics and phototochemistry have been widely investigated experimentally both in the protein and in solution.[2−6] Changes in P_r/P_{fr} spectral properties are usually assigned to an initial $Z \rightarrow E$ photoisomerization of the C15═C16 double bond, which leads to the Lumi-R intermediate within few tens of picoseconds,[7,8] and a subsequent isomerization of the adjacent single bond C14−C15, although the latter has been recently questioned on the basis of new evidence that either favors another rotation at the A−B bridge[9,10] or even rules out any other isomerization but the photochemical one.[11,12] The primary photoinduced event has been shown to follow the same complex multiexponential kinetics both in the protein and in solvent, with a fast (about 2−3 ps) and a slow (about 30−40 ps) component, suggesting a similar deactivation mechanism regardless the environment. Interestingly, it has been recently shown (via combined vis/vis and vis/IR pump/probe experiments)[7] that only

SCHEME 1: Phytochromes Photocycle

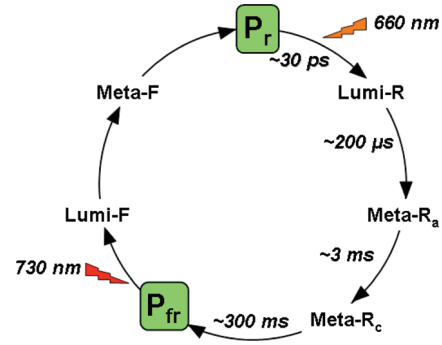

SCHEME 2: Phys Chromophores: Phytochromobilin (PΦB), Biliverdin (BV), and Phycocyanobilin (PCB)[a]

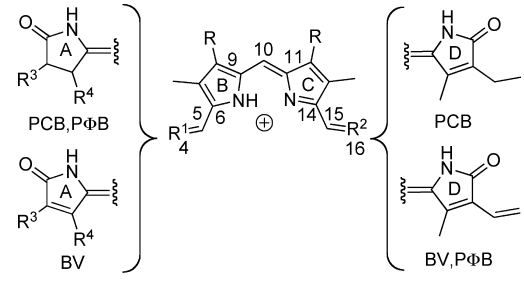

[a] The tetrapyrrolic model system employed has been simplified by replacing R, R^3, and R^4 with H.

* To whom correspondence should be addressed. For M.M.: e-mail, Manuela.Merchan@uv.es. For M.G.: e-mail, marco.garavelli@unibo.it.

[†] Università di Bologna.

[‡] Universitat de València.

[§] Imperial College London.

10.1021/jp904669x CCC: $40.75
Published on Web 07/09/2009

the slow (>30 ps) component is the photoreactive one leading to C15=C16 photoisomerization (and Lumi-R) with a rather small quantum yield (~9%) that nicely matches the one found for P_{fr} formation (~8%).[13] Notably, it has been suggested[7] that the isomerization occurs within the lifetime of S_1 (for which an even shorter decay component (0.7 ps) was detected), although a multistep process that is initiated in the excited state and, eventually, is finalized on S_0 cannot be ruled out. Indication of a C15=C16 $Z \rightarrow E$ photoisomerization that is complete on the excited state surface is also supported by very recent femtosecond stimulated Raman spectroscopies.[14] These results suggest initial formation (within 0.6 ps) of a predistorted excited state intermediate (I*), followed by formation (in ~3 ps) of a later excited state Lumi-R-like photoproduct (Lumi-R*), where C15=C16 isomerization has been mostly finalized.

Despite the several ultrafast time-resolved spectroscopic studies, the primary events holding the key to photon energy storage and photocycle initiation remain obscure. Computational photochemistry[15,16] would provide the way for a molecular scale understanding of those fast events, as it offers the tools for analyzing the details of the photoinduced molecular motion. Because of the complexity and size of the system, few computational studies have appeared[17−19] and details of the photoinduced molecular motion and decay mechanism are still uncertain. In order to elucidate these processes, energy profiles for excited state relaxation paths have been investigated for a bare cationic PΦB model in vacuo via high level ab initio correlated (CASPT2) methods. Competitive deactivation routes emerge that unveil the primary photochemical event and the intrinsic photoisomerization ability of phys chromophores and suggest a qualitative rationale for the multiexponential decay and short (picosecond) excited state lifetime observed.[6] Spectroscopic properties have been also simulated in both isolated conditions and the protein (via a QM and QM/MM approach, respectively) that satisfactorily match (within a 4 kcal/mol error) experimental data.

2. Methodology

Molecular Model Selection. To reduce computational complexity and cost, a simplified tetrapyrrolic choromophore has been selected as the PΦB model: the thioether, the methyl groups on the ring A, and the propionic carboxyl groups are replaced by hydrogen atoms (see Scheme 2). A ZZZasa chromophore geometry is assumed in this work (see Scheme 2) as suggested by several spectroscopic experiments in phys.[20] Anyway, it must be pointed out that the initial conformation for the chromophore in the protein is still widely under discussion, as good arguments of vibrational spectroscopy for both a ZZZasa and a ZZZssa structure have been presented.[1,4] Furthermore, the chromophore is likely to adopt a cyclic (or helical) porphyrin-like ZZZsss geometry when free in solution.[1,21] Despite the specific conformation selected in this work, the photoisomerization processes documented below are considered to be unaffected by the geometry adopted, as these isomerizations are all one-bond-flip events that are highly independent of the stereochemistry of other bonds, and the presented results are suggested to have a more general flavor.

Computational Methods: Selection and Validation. To select and validate the computational approach adopted for geometry optimization and energy evaluation, a full arsenal of different computational methods (such as HF, MP2, DFT, CIS, RASSCF, CASSCF, CASPT2, and RICC2) have been used and the results compared. Briefly (details of this analysis are reported in the subsections below and Supporting Info (SI)), ground (S_0) and excited state (S_1) geometry optimizations are carried out using Gaussian03[22] at the MP2 and CIS levels, respectively, whereas all energies are reevaluated at the CASPT2[23] level with MOLCAS 6.0[24] to account for correlation effects and to compute accurate energy profiles and spectroscopic properties. A 6-31G(d) basis set is employed throughout as a compromise between computational cost and reliability of the results; because of the size of the PΦB model employed, any larger (although more reliable) basis set would be too demanding.

Ground State Optimizations. Ground state geometry optimization has been performed according to different methods, namely, HF, MP2, DFT/B3LYP, and CASSCF. While application of HF/MP2/DFT methods is straightforward, the choice of the active space is critical for CASSCF computations. Unfortunately, in a system as large as PΦB, it is not possible to include the full π system (28 electrons in 25 π orbitals), and it must be drastically reduced. An 8 electrons/8 orbitals active π space has been initially selected and used for CASSCF(8,8) geometry optimizations. This comprises the last three π occupied HF orbitals and the first three π^* virtual HF orbitals (that are all located on the central B and C rings) and the two π/π^* orbitals describing the C15=C16 double bond (i.e., the biologically active one involved in the photoisomerization). Unfortunately, it is apparent that this choice is not perfectly balanced (i.e., the active space is not uniformly/symmetrically distributed on the tetrapyrrolic system): it biases C15=C16 photoisomerization, and it may create some problems for the correct geometrical description of the system during CASSCF geometry optimizations as some regions are better described than others, which may result in unrealistic asymmetries of the optimized structures. Thus, to avoid this problem, also a 12 electrons/11 orbitals active π space has been used for a RASSCF(12,11) (where all single and double excitations within the active space have been considered) geometry optimization, which is perfectly balanced and uniformly distributed on the tetrapyrrolic system: four electrons in the four π/π^* orbitals describing the C4=C5 and C15=C16 double bonds, plus eight electrons in the seven π/π^* orbitals of the central ($B_{ring}-C_{10}H-C_{ring}$) part of PΦB.

While a delocalized resonance-hybrid appears as the unique stable ground state structure at the HF, MP2, and DFT/B3LYP levels (with the three methods substantially returning a similar structure where the positive charge is equally shared between the B and C rings), both CASSCF(8,8) and RASSCF(12,11) do produce a two-minima ground state topology, with the two stable geometries corresponding to the two localized resonant Lewis structures (and the positive charge that is localized either on one (B) or on the other (C) of the two central rings), regardless the active space used in MC-SCF computations (see Table S1 in SI for geometrical parameters). These results shed some doubts on the reliability of MC-SCF geometries, perhaps because of the reduced active space we are forced to use or because dynamic correlation becomes crucial (and must be accounted for) to describe delocalization effects. This is typical for systems (such as PΦB) where there is a competition between localized and delocalized resonant structures. In this case, it is well-known that inclusion of dynamic correlation normally favors the more equalized structure. For instance, ground-state free base porphin has a D_{2h} geometry at the MP2 level, whereas lower level computations lead to a C_{2v} structure.[25,26]

To further validate this delocalized picture, single-point ground-state CASPT2 computations have been also performed on top of the MP2 and CASSCF optimized structures to have a homogeneous and uniform set of accurate correlated energies (see Table S2 in SI for absolute energy values). These

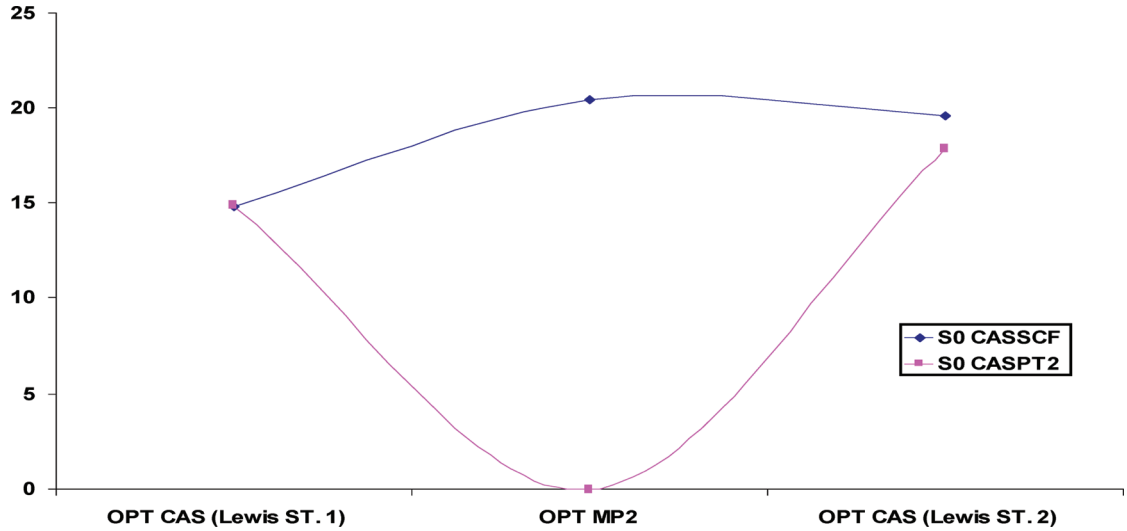

Figure 1. CASSCF and CASPT2 energy profiles (kcal/mol) connecting CASSCF and MP2 ground state minima.

calculations substantially confirm the single minimum MP2 topology (which is also apparent at the HF and DFT level): the optimized resonance-hybrid MP2 geometry appears at least 15 kcal/mol lower in energy than the two localized CASSCF minima (see Figure 1), thus clearly ruling out CASSCF ground state structures and calling for the delocalized resonance-hybrid as the real minimum in the ground state.

Excited State Optimizations. The problems experienced by CASSCF for S_0 geometry optimizations do suggest that CASSCF is perhaps not a suitable choice for excited state optimizations as well. Unfortunately, methods capable of performing excited state geometry optimization at the highly correlated level are scarce[27] and they certainly become technically impracticable for a system of the molecular size as the chromophore under study, especially for determination of conical intersections. As it has been documented for DNA nucleobases, upon geometry optimization the CIS method yields directly to the S_1/S_0 CI of DNA/RNA nucleobases. This has been subsequently confirmed by using higher-level methodologies.[28] Thus, inspired by (i) those findings, (ii) the fact that the HF approach (that is its ground state counterpart) does also appear to work properly on the ground state (HF accounts for the correct resonance-hybrid structure, delivering a geometry that is very close to the MP2 one; see discussion above), and (iii) the almost pure single (HOMO → LUMO) excitation character of the S_1 state, the CIS approach has been selected for preliminary geometry determinations on the lowest excited state S_1 of the PΦB model. This choice is further supported by CASPT2 calibration computations on optimized PΦB structures, showing that S_1 CIS optimized geometries do work better (i.e., they always return a lower CASPT2 energy) than the corresponding CASSCF optimized structures. Thus, quite surprisingly and unexpectedly, it is concluded that CASSCF does not represent a reliable method for geometry optimization in this case, neither in the ground nor in the excited state, while CIS is capable of mimicking the work of high-level geometry determinations, even though it does not account for electron correlation. In summary, different structures belonging to the S_1 hypersurface have been characterized at the CIS level, just as a practical computational strategy and after a careful analysis of other alternative computational approaches, including the much more expensive CASSCF approach.

Ground and Excited State Energy Estimates. On top of the optimized ground/excited state structures, single point CASPT2 computations have been employed to account for correlation energy and compute accurate energy differences (see Tables S3 and S4 in SI for absolute energy values). The successful performance of CASPT2 in computing experimentally accurate energies (with errors usually below 4 kcal/mol) and spectroscopic properties is well-established and is the reason for using this method in evaluating the ground and excited state energies of the investigated system.

The choice of the active space is critical for CASPT2. Unfortunately, in a system as large as PΦB, it is not possible to include the full π system, which is composed of 28 electrons in 25 orbitals, and a calibration is needed in order to select the proper reduced active space. For this purpose, the optimized ground-state MP2/6-31G(d) geometry computed for the tetrapyrrolic model designed was used. The selection of the active space has been performed by analyzing the convergence of the vertical spectroscopic properties (transition energies and related oscillator strengths) upon a systematic increasing of the number of active orbitals and active electrons (see Table S5 in SI). A 11 π/π^* orbitals, 10 electrons active space, joined to a three-roots state average procedure, leads to CASSCF/CASPT2(11,10) results that can be considered in practice to be converged within the error bars of the method (see SI for details). The standard zeroth-order Hamiltonian was employed in the CASPT2 calculations, which include an imaginary level-shift correction of 0.2 au in order to avoid the presence of intruder states. The CASSCF state interaction (CASSI) method[29] was used (as implemented in MOLCAS 6.0[24]) to calculate the transition dipole moments from the reference zeroth-order CASSCF wave function. The latter moments were used, together with CASPT2 corrected energies, to compute oscillator strengths (f). These data unambiguously reveal that the single HOMO → LUMO excitation state S_1 is the bright state, in agreement with all the other methods employed.

Finally, multireference (i.e., CASPT2) and single reference (i.e., TD-RICC2) correlated energies have been compared at all the points of the investigated channels. This is done to access the validity of a multireference perturbation vs a single reference-CC2 approach and disclose the reliability of the selected protocol for energy estimates. Because of the relevant charge transfer character along the photoisomerization paths (see the results below), TD-RICC2 appears unsuitable for the

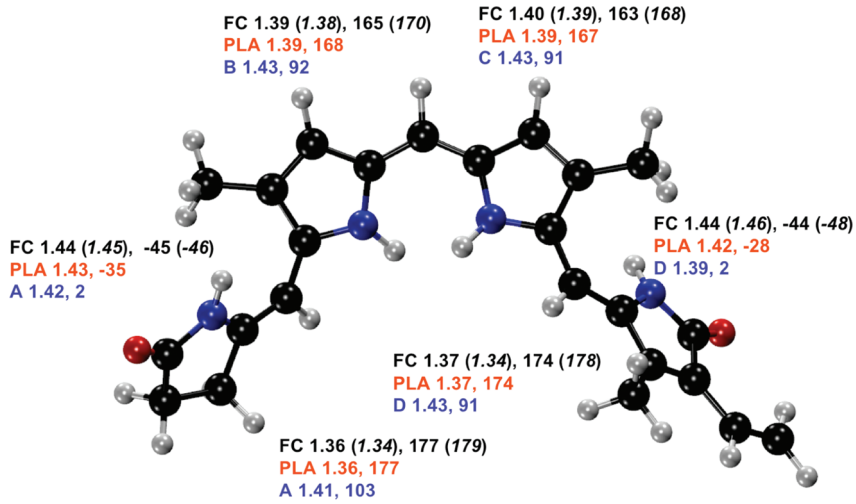

Figure 2. Relevant geometrical parameters (bonds in Å and twisting angles in degrees) computed for the MP2 and HF (numbers in italics) optimized ground state minimum (FC) and the CIS optimized excited state minima (PLA, A, B, C, D). The molecular geometry reported corresponds to the FC one.

description of the photoisomerization processes and CASPT2 turns out to be the most reliable choice (see SI for further details).

QM/MM Computations. Hybrid QM/MM computations in the protein (the resolved phys structure 1ZTU[11] has been used, as it was the only one available when we started this investigation) have been performed employing our recently developed COBRAMM interface[30] that combines AMBER8[31] and Gaussian[22] and accounts for chromophore/protein electrostatic interactions at the highest (QM) level by employing an electrostatic embedding scheme. Details of this hybrid approach are presented elsewhere. Briefly, the method is based on a hydrogen link−atom scheme.[32] QM and MM layers interact in the following ways: (i) all QM atoms feel the electrostatic potential of all MM point charges (i.e., an electrostatic embedding scheme has been adopted); (ii) all the bonding (i.e., stretching, bending, and torsion) and the van der Waals QM/MM cross-terms are described by the standard MM potential; (iii) electrostatic interactions involving MM atoms are all accounted for classically.

The QM region is represented by the chromophore atoms (note that the cromophore is BV rather than PΦB in the available crystallographic structure) except its two propionic groups that are included in the MM region comprising also the crystallographic waters and the rest of the protein. The same QM approach as described above for PΦB in vacuo is used for BV, while the ff99 force field[31] is employed for the surrounding MM region. The cromophore atoms, the two water molecules HOH12 and HOH18, and the side chain of the LYS24, which is covalently linked to the QM part, are left free to move, while all the rest is kept frozen at its crystallographic position during all calculations. Using the standard Amber package tools the protein has been solvated with a water cup centered on BV and with a 20 Å radius. The hydrogen atoms, lacking in the crystallographic structure, have been added using the H++[33] program. The protonation state of the residues close to the chromophore (HIS260, ASP207, HIS290) and the orientation of HOH12 and HOH18 have been corrected in order to preserve the hydrogen bond network previously documented.[11] In order to minimize spurious steric interactions between nearby protein residues and BV, residues within 10 Å around the chromophore have been preoptimized at the MM (ff99) level.

To account for correlation energy, CASPT2 computations are performed on top of the optimized points in the bath of the protein (AMBER) point charges by adopting the same procedure described above for PΦB in vacuo.

Further details on the method and protein setup are reported in the SI.

3. Results and Discussion

As depicted in Figure 2, the ground state minimum at the Franck−Condon region (called FC thereafter) (which is slightly twisted to minimize steric interactions due to the rings substituents) appears as a stable resonance-hybrid where the positive charge is equally shared by B and C rings. Its structure is roughly symmetric with respect to the central carbon atom C10. These properties are conserved in the relaxed, roughly planar excited state structure (S_1 minimum, called PLA thereafter), where a rearrangement in the skeletal bonds occurs (a maximum difference of 0.04 Å is seen for HF → CIS C14−C15 bond shortening; see Figure 2).

The S_1 state is mainly described by the singly excited configuration HOMO → LUMO, with both orbitals delocalized in the two central (B, C) rings and exocyclic (C4−C5, C15−C16) bonds, leaving unaffected the external (A, D) rings (see Figure S1 in the SI). Thus, the electronic transition has no effect on the dipole moment of the molecule because the two orbitals share the same spatial region and no intramolecular charge transfer takes place at FC and PLA. The calculated vertical $S_0 \rightarrow S_1$ absorption energy is in reasonable agreement with the experimental values recorded both in solution[34] and in phys[35] (see Table 1). It is noted that the conformation of the chromophore in solution may be different (ZZZsss) from the one considered here (ZZZasa, as suggested in phys[20]). However, since the excitation is located at the center of the chromophore that is structurally preserved in the two conformers, the effects on transition energies are expected to be minor and fall well within the error of the employed computational approach. The S_1 minimum (PLA) produced by the initial excited state dynamics out of the Franck−Condon region may be assigned reasonably to the emitting state: here, it is where the system gets funneled following absorption and stands for a while before internal vibrational energy redistribution occurs and deactivation channels leading to ground state recovery are populated. In this sense, it is worth mentioning that the $S_1 \rightarrow S_0$ vertical energy

TABLE 1: Absorption and Emission Features Computed in Vacuo and in the Protein (λ in nm)[a]

	PΦB			protein (BV)	
	CASPT2	exptl		CASPT2	
abs/em	(vacuo)	solvent[b]	protein[c]	(QM/MM)	Exp.
λ_{abs}	642	590	666	709	700[d]
λ_{em}	673	680−690	685	742	*e*

[a] Experimental values are also reported. [b] Reference 34: The dihydrobiliverdin chromophore in CH_3Cl solution slightly differs from PΦB, as it contains a methoxycarbonylmethyl substituent at C3 and an ethyl group, rather than a vinyl, at C18. This may partly account for the blue-shifted value. [c] Spectra recorded in a PΦB containing phytochrome; see ref 35. [d] Reference 36. [e] Not detected in BV containing phys.

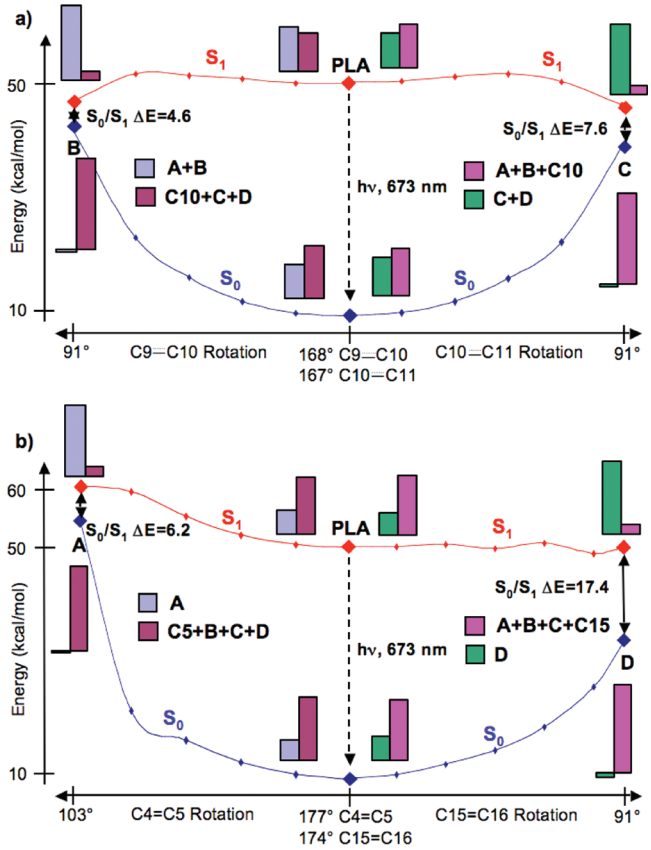

Figure 3. CIS-relaxed scans along the four torsional modes. The starting (PLA) and twisted ending points (part a, paths B and C; part b, paths A and D) are CIS fully optimized minima. Energy profiles are recalculated at the CASPT2 level (i.e., CASPT2 energy corrections are performed on top of all the points along the four paths). The amount of positive charge carried by each rotating fragment is displayed in bar diagrams (Mulliken charges as from the zeroth-order CASSCF wave function are considered) and underscores the charge transfer character of the electronic state.

gap computed at PLA matches the emission wavelength observed for the chromophore in the different environments (see Table 1).

PLA appears as a transient located on a very flat region of the S_1 potential energy surface. In particular, four possible one-bond-flip isomerization paths have been mapped to escape PLA, each one involving the twisting of one specific exocyclic bond: C4−C5 (path A), C9−C10 (path B), C10−C11 (path C), and C15−C16 (path D); see Figure 3. Three of them are competitive, almost barrierless, isomerization channels (paths B, C, and D with activation energies of 1.9, 1.5, and 0.7 kcal/mol, respectively), while a fourth path (A) is unfavored (ending at a point on S_1 that is 15.7 kcal/mol higher than PLA). Interestingly, the S_1-S_0 energy gaps at the twisted (ending) points of paths B and C are rather small (only 5 and 8 kcal/mol, respectively). On the other hand, and rather surprisingly, the S_0-S_1 energy gap at the twisted minimum along the biologically active path D (involving the isomerization of the C15=C16 bond) is much larger (17.4 kcal/mol). Charge analysis reveals that whereas no significant intramolecular charge transfer takes place at FC and PLA for S_1 (HOMO → LUMO) and the excitation stays mainly localized at the center of the chromophore, the positive charge progressively moves and gets localized into the shortest twisted half, and a pure twisted intramolecular charge transfer (TICT) state appears at the twisted optimized points (see Figure 3). These results clearly rule out computational approaches that do not satisfactorily account for photoinduced charge transfers (such as TD-DFT with standard functionals).[37] A TD-DFT/b3lyp computational study has recently appeared[19] reporting results for the photoinduced molecular motion of a PΦB model that are seemingly consistent with the present work (path D is less favored than path B/C), although for different reasons; a barrier appears along path D, while paths B/C are substantially barrierless. Additionally, CIs and efficient deactivation channels have not been located. It is doubtful wether TD-DFT/b3lyp can give reliable results along the photoisomerization paths, specifically when highly twisted structures are explored, because of the above-mentioned charge transfer character characterizing the twisted region. Thus, while such an approach may deliver some insight into the photoinduced motion at planar (or nearly planar) structures, attention must be paid not to overinterpret reaction barriers that occur along the isomerization paths at highly twisted geometries.

Considering the small CASPT2 S_1-S_0 energy gap at the twisted minima B and C, it is suggested that these points are (or are close to) conical intersection (CI) funnels, whereas the energy gap at D seems far too large (at least at this level, vide infra) to support the existence of a CI at this point. Thus, according to the CASPT2//CIS results, a deactivation scheme emerges for isolated PΦB with multiple competitive internal conversion (IC) routes: two photoisomerization paths (B and C) leading to ultrafast decay through directly accessed twisted CIs and a third one (D) populating a twisted excited state minimum and, possibly, a nearby CI related to a slower IC (see below). Interestingly, this isolated molecule model, displaying easily accessible twisted minima and/or CIs, can qualitatively account for most of the properties recorded in both solvents and the proteins, namely, the ultrafast (picosecond) decay of the emission, its rather small quantum yield (QY, $\sim 10^{-3}$), the short S_1 lifetime, its multiexponential decay, the faster (2−3 ps)[6] lifetime component that is here related to paths B and C, and the slow (>30 ps) component that has been shown to be related to C15=C16 photoisomerization[7] (i.e., path D). Since the observed multiexponential decay and transient spectroscopic features are the same regardless of the environment (i.e., solvent or protein), this reactive scheme is tentatively suggested to be a more general model for the photobehavior of phys chromophores.

It must be pointed out that the viability of the slow (but still ultrafast, i.e., tens of picoseconds long)[7,8] component via path D depends on the existence and accessibility of a CI from the twisted minimum on S_1, as the S_1-S_0 energy gap documented here at the CASPT2//CIS level is inconsistent with a ~30 ps decay. We believe that a CI exists and is close in energy and geometry to the twisted D minimum and that the surprisingly

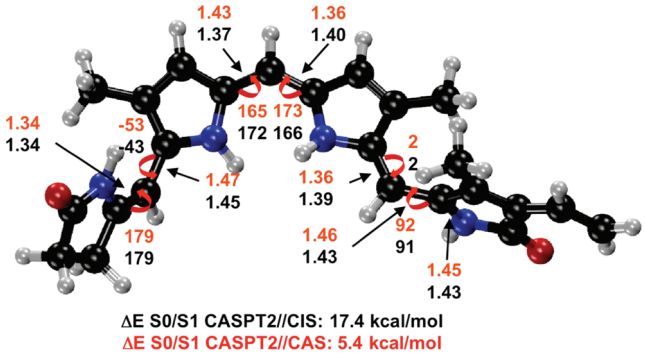

Figure 4. Relevant geometrical parameters (bonds in Å and twisting angles in degrees) for the twisted point D optimized on S_1 at both the CIS (black values) and CASSCF (red values) levels. The CASPT2 S_0-S_1 energy gap is also highlighted.

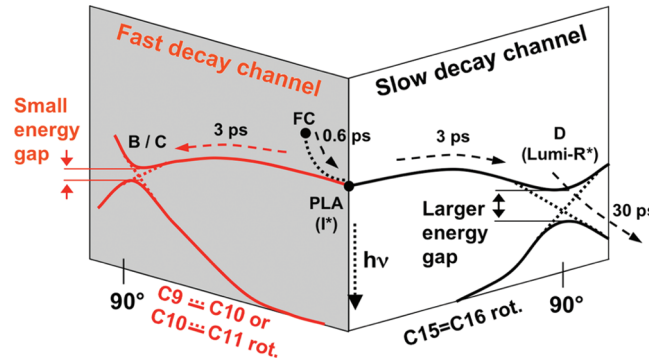

Figure 5. Schematic representation of competitive photoreaction paths in phys chromophores according to the CASPT2//CIS scenario. Decay time components from experimental data[7,8,14] are also tentatively assigned to the corresponding reaction routes. PLA is assigned to the early (i.e., subpicosecond time scale formation) excited state intermediate (I*) and D to the later (i.e., 3 ps time scale formation) excited state intermediate (Lumi-R*) observed in ref 14. Decay from D is assigned to the slower (~30 ps) deactivation component, while the biologically inactive paths B and C drive the fast (3 ps) and main depletion of the excited state. This also accounts for the smaller QY observed through path D and the decrease in the intensity of the signal associated with the corresponding vibrational signatures.[14]

large S_1-S_0 energy gap at this point is a clue to a local deficiency in the CIS approach employed for the optimization of the twisted highly deconjugated structure D. Our conviction is based on the similarity of paths A and D that are indeed structurally and chemically nearly equivalent: as the former path ends into a sloped-type CI (see Figure 3), we think that the same holds for path D. It is also reminded that the S_1-S_0 energy gap at the twisted D minimum is certainly overestimated, as CIS optimizations do not include dynamic correlation effects and are known to undervalue the elongation of the twisted double bonds (C15═C16 bond is 1.43 Å; see Figure 2), leading to artificial enlargement of the energy gap at these geometries. Very remarkably, the CASPT2 S_0-S_1 energy difference is reduced to only 5.4 kcal/mol at the reoptimized CASSCF(10,11) twisted point where the C15═C16 bond is longer (1.46 Å; see Figure 4). As outlined in the computational methods section, CASSCF-based optimizations cannot be reliably used for a systematic exploration of the surface. Nevertheless, here we apply this approach to the twisted D structure where deconjugation, and the concurrent localization of the excitation (see discussion above), occurs. Thus, failure of CASSCF in describing extended delocalized structures (such as the planar resonance hybrids) is expected to be minor here. The reliability of the CASSCF twisted structure is also supported by its CASPT2 S_1 energy that is lower than that of the corresponding CIS geometry. This final evidence further supports our conjectures and suggests that the excited twisted minimum D is close to a real crossing, as it has been already found for A.

In summary, the valuable information for this chromophore to append to its intrinsic photophysics/photochemistry is that competitive almost barrierless isomerization routes exist that lead to TICT CI or minima where equilibration occurs and thus provide a qualitative rationale for the observed ultrafast multiexponential decay. While this is a well-established result of our investigation, we tentatively suggest (according to CASPT2//CIS results) that the slow (fast) decay component is due to deactivation through path D (B/C), as described before, and that the early excited intermediate recently observed in phys within 0.6 ps (I*)[14] corresponds to PLA (where initial distortion of the C14−C15═C16 moiety occurs), while the late excited intermediate formed in 3 ps (Lumi-R*)[14] corresponds to the highly twisted minimum D optimized on S_1 that is a precursor of the Lumi-R photoproduct (see Figure 5). A final statement on all these points will be accessible only when reliable correlated methods (e.g., MR-MP2) for topological/dynamical analysis of the excited state of phys chromophores will become available, which is yet far from realization, unfortunately.

While inspection of the available crystal structures of the phys chromophore domain[11] points out that full C9−C10 and C10−C11 isomerizations cannot occur in the protein, here we suggest that those twistings may initiate on S_1 (when they are not yet too space demanding and when concurrent hula-twist/bicycle-pedal motions may possibly assist them), thus activating the fast IC component through the twisted funnels; however, they cannot be completed on S_0 (because of their volume demand) and get aborted (i.e., reactant back formation occurs). On the other hand, path D has enough space to be finalized on S_0, although with a longer time scale and a small QY (~9%).[7] Validation of this hypothesis is far beyond the scope of this work, as it would involve mapping the photoisomerization channels into the protein by using, for instance, QM/MM methods. Here, we just show how our preliminary QM/MM computations in the protein satisfactorily reproduce the spectroscopic (absorption and emission) features observed in phys (see Table 1). The QM/MM optimized ground/excited state BV is a hybrid resonance structure similar to the PΦB model previously optimized in vacuo. The calculated vertical absorption is in striking agreement with the value recorded in the protein[36] (see Table 1), thus supporting the reliability of this model. Protein emission (following direct S_1 excitation) has not yet been detected in BV containing proteins, while only a very weak emission has been recorded for PΦB in phys (see Table 1),[38−40] indicating that this is a very unfavored process and that very efficient IC routes must be already active. We suggest these to be aborted isomerizations through paths B and C (see Figure 5).

4. Conclusions

This study underscores the importance of competitive isomerization routes in the photoreactivity of a realistic phys chromophore model in vacuo. These paths drive the system into twisted intramolecular charge transfer minima/conical intersections, thus accounting for an ultrafast radiationless multiexponential/multichannel decay. Eventually, this study delivers a model for the intrinsic photochemical behavior of phys chromophores that also succeeds in providing a qualitative rationale for the observed behavior in solvent and protein. Spectroscopic

features are reproduced, and the agreement with the available experimental data is satisfactory. This supports the adequacy of the computational approach and model systems employed and the reliability of the drawn photoreactivity scheme, at least on a qualitative ground.

Acknowledgment. Financial support is acknowledged from MURST PRIN 2005, Projects CompRenDe (Bologna University), CTQ2007-61260, and CSD2007-0010 Consolider-Ingenio in Molecular Nanoscience of the Spanish MEC/FEDER. M.G. and P.A. thank E4-Computer Engineering Spa for granted computational time and technical assistance.

Supporting Information Available: Analysis of methods, MO, QM/MM details and protein setup, geometries, and energies. This material is available free of charge via the Internet at http://pubs.acs.org.

References and Notes

(1) Rockwell, N. C.; Su, Y.-S.; Lagarias, J. C. *Annu. Rev. Plant Biol.* **2006**, *57*, 837.

(2) Schaffner, K.; Braslavsky, S. E.; Holzwarth, A. R. Protein Environment and Photophysics and Photochemistry of the Prosthetic Chromophores of Biliproteins. In *Frontiers in Supramolecular Organic Chemistry and Photochemistry*; Schneider, H.-J., Dürr, H., Eds.; VCH Verlagsgesellschaft: Weinheim, Germany, 1991.

(3) Holzwarth, A. R.; Venuti, E.; Braslavsky, S. E.; Schaffner, K. *Biochim. Biophys. Acta* **1992**, *1140*, 59.

(4) Gärtner, W.; Braslavsky, S. E. The Phytochromes: Spectroscopy and Function. In *Photoreceptors and Light Signaling*; Batschauer, A., Ed.; Royal Society of Chemistry: Cambridge, U.K., 2004; Vol. 3, pp 136−180.

(5) Falk, H. *The Chemistry of Linear Oligopyrroles and Bile Pigments*; Springer-Verlag: New York, 1989.

(6) Rentsch, S.; Hermann, G.; Bischoff, M.; Strehlow, D.; Rentsch, M. *Photochem. Photobiol.* **1997**, *66*, 585.

(7) Schumann, C.; Groβ, R.; Michael, N.; Lamparter, T.; Diller, R. *ChemPhysChem* **2007**, *8*, 1657.

(8) Müller, M. G.; Lindner, I.; Martin, I.; Gärtner, W.; Holzwarth, A. R. *Biophys. J.* **2008**, *94*, 4370.

(9) Mroginski, M. A.; Murgida, D. H.; Hildebrandt, P. *Acc. Chem. Res.* **2007**, *40*, 258.

(10) Thor, J. J. v.; Ronayne, K. L.; Towrie, M. *J. Am. Chem. Soc.* **2007**, *129*, 126.

(11) Wagner, J. R.; Brunzelle, J. S.; Forest, K. T.; Vierstra, R. D. *Nature* **2005**, *438*, 325.

(12) Inomata, K.; Hammam, M. A. S.; Kinoshita, H.; Murata, Y.; Khawn, H.; Noack, S.; Michael, N.; Lamparter, T. *J. Biol. Chem.* **2005**, *280*, 24491.

(13) Hughes, J.; Lamparter, T.; Mittmann, F.; Hartmann, E.; Gartner, W.; Wilde, A.; Borner, T. *Nature* **1997**, *386*, 663.

(14) Dasgupta, J.; Frontiera, R. R.; Taylor, K. C.; Lagarias, J. C.; Mathies, R. A. *Proc. Natl. Acad. Sci. U.S.A.* **2009**, *106*, 1784.

(15) Olivucci, M. *Computational Photochemistry*; Elsevier: Amsterdam, 2005; Vol. 16.

(16) Domcke, W.; Yarkony, D.; Köppel, H. *Conical Intersections: Electronic Structure, Dynamics & Spectroscopy*; World Scientific: Singapore, 2004.

(17) Durbeej, B.; Eriksson, L. A. *Phys. Chem. Chem. Phys.* **2006**, *8*, 4053.

(18) Borg, O. A.; Durbeej, B. *Phys. Chem. Chem. Phys.* **2008**, *10*, 2528.

(19) Durbeej, B. *Phys. Chem. Chem. Phys.* **2009**, *11*, 1354.

(20) Kneip, C.; Hildebrandt, P.; Schlamann, W.; Braslavsky, S. E.; Mark, F.; Schaffner, K. *Biochemistry* **1999**, *38*, 15185.

(21) Knipp, B.; Müller, M.; Metzler-Nolte, N.; Balaban, T. S.; Braslavsky, S. E.; Schaffner, K. *Helv. Chim. Acta* **1998**, *81*, 881.

(22) Frisch, M. J.; Trucks, G. W.; Schlegel, H. B.; Scuseria, G. E.; Robb, M. A.; Cheeseman, J. R.; Montgomery, J. A., Jr.; Vreven, T.; Kudin, K. N.; Burant, J. C.; Millam, J. M.; Iyengar, S. S.; Tomasi, J.; Barone, V.; Mennucci, B.; Cossi, M.; Scalmani, G.; Rega, N.; Petersson, G. A.; Nakatsuji, H.; Hada, M.; Ehara, M.; Toyota, K.; Fukuda, R.; Hasegawa, J.; Ishida, M.; Nakajima, T.; Honda, Y.; Kitao, O.; Nakai, H.; Klene, M.; Li, X.; Knox, J. E.; Hratchian, H. P.; Cross, J. B.; Bakken, V.; Adamo, C.; Jaramillo, J.; Gomperts, R.; Stratmann, R. E.; Yazyev, O.; Austin, A. J.; Cammi, R.; Pomelli, C.; Ochterski, J. W.; Ayala, P. Y.; Morokuma, K.; Voth, G. A.; Salvador, P.; Dannenberg, J. J.; Zakrzewski, V. G.; Dapprich, S.; Daniels, A. D.; Strain, M. C.; Farkas, O.; Malick, D. K.; Rabuck, A. D.; Raghavachari, K.; Foresman, J. B.; Ortiz, J. V.; Cui, Q.; Baboul, A. G.; Clifford, S.; Cioslowski, J.; Stefanov, B. B.; Liu, G.; Liashenko, A.; Piskorz, P.; Komaromi, I.; Martin, R. L.; Fox, D. J.; Keith, T.; Al-Laham, M. A.; Peng, C. Y.; Nanayakkara, A.; Challacombe, M.; Gill, P. M. W.; Johnson, B.; Chen, W.; Wong, M. W.; Gonzalez, C.; Pople, J. A. *Gaussian 03*, revision C.02; Gaussian, Inc.: Wallingford, CT, 2004.

(23) Andersson, K.; Malmqvist, P. A.; Roos, B. O. *J. Chem. Phys.* **1992**, *96*, 1218.

(24) Andersson, K.; Barysz, M.; Bernhardsson, A.; Blomberg, M. R. A.; Carissan, Y.; Cooper, D. L.; Cossi, M.; Fülscher, M. P.; Gagliardi, L.; de Graaf, C.; Hess, B.; Hagberg, G.; Karlström, G.; Lindh, R.; Malmqvist, P.-Å.; Nakajima, T.; Neogrády, P.; Olsen, J.; Raab, J.; Roos, B. O.; Ryde, U.; Schimmelpfennig, B.; Schütz, M.; Seijo, L.; Serrano-Andrés, L.; Siegbahn, P. E. M.; Stålring, J.; Thorsteinsson, T.; Veryazov, V.; Widmark, P. O. *MOLCAS 6.0*; Department of Theoretical Chemistry, Chemical Centre, University of Lund: Lund, Sweden, 2004.

(25) Almlöf, J.; Fischer, T. H.; Gassman, P. G.; Ghosh, A.; Häser, M. *J. Phys. Chem.* **1993**, *97*, 10964.

(26) Merchán, M.; Ortí, E.; Roos, B. O. *Chem. Phys. Lett.* **1994**, *221*, 136.

(27) Merchán, M.; Serrano-Andrés, L. *THEOCHEM* **2005**, *729*, 99.

(28) Merchán, M.; Gonzalez-Luque, R.; Climent, T.; Serrano-Andrés, L.; Rodríguez, E.; Reguero, M.; Pelaez, D. *J. Phys. Chem. B* **2006**, *110*, 26471.

(29) Malmqvist, P.-Å.; Roos, B. O. *Chem. Phys. Lett.* **1989**, *155*, 189.

(30) Altoè, P.; Stenta, M.; Bottoni, A.; Garavelli, M. *Theor. Chem. Acc.* **2007**, *118*, 219.

(31) Case, D. A.; Cheatham, T. E.; Darden, T.; Gohlke, H.; Luo, R.; Merz, K. M.; Onufriev, A.; Simmerling, C.; Wang, B.; Woods, R. J. *J. Comput. Chem.* **2005**, *26*, 1668.

(32) Singh, U. C.; Kollman, P. A. *J. Comput. Chem.* **1986**, *7*, 718.

(33) Gordon, J. C.; Myers, J. B.; Folta, T.; Shoja, V.; Heath, L. S.; Onufriev, A. *Nucleic Acids Res.* **2005**, *33*, 368.

(34) Ditto, M.; Brunner, H.; Lippitsch, M. E. *Chem. Phys. Lett.* **1991**, *185*, 61.

(35) Büchler, R.; Hermann, G.; Lap, D. V.; Rentsch, S. *Chem. Phys. Lett.* **1995**, *233*, 514.

(36) Wagner, J. R.; Zhang, J.; von Stetten, D.; Gunther, M.; Murgida, D. H.; Mroginski, M. A.; Walker, J. M.; Forest, K. T.; Hildebrandt, P.; Vierstra, R. D. *J. Biol. Chem.* **2008**, *283*, 12212.

(37) Dreuw, A.; Head-Gordon, M. *J. Am. Chem. Soc.* **2004**, *126*, 4007.

(38) Sineshchekov, V.; Ogorodnikova, O.; Thiele, A.; Gatz, C. *J. Photochem. Photobiol., B* **2000**, *59*, 139.

(39) Sineshchekov, V. A.; Ogorodnikova, O. B.; Devlin, P. F.; Whitelam, G. C. *J. Photochem. Photobiol., B* **1998**, *42*, 133.

(40) Sineshchekov, V. A.; Ogorodnikova, O. B.; Weller, J. L. *J. Photochem. Photobiol., B* **1999**, *49*, 204.

JP904669X